Journal of Mechanics in Medicine and Biology
Vol. 14, No. 3 (2014) 1450033 (18 pages)

DOI: 10.1142/S021951941450033X

World Scientific
www.worldscientific.com

A STRUCTURE-MOTIVATED MODEL OF THE PASSIVE MECHANICAL RESPONSE OF THE PRIMARY PORCINE RENAL ARTERY

BORAN ZHOU*, LAUREN WOLF*, ALEXANDER RACHEV*
and TAREK SHAZLY*,†,‡

*College of Engineering and Computing
Biomedical Engineering Program
University of South Carolina
Columbia, SC, 29208, USA

†College of Engineering and Computing
Mechanical Engineering Department
University of South Carolina
Columbia, SC, 29208, USA
‡shazly@engr.sc.edu

Received 10 June 2013
Revised 1 October 2013
Accepted 16 October 2013
Published 12 December 2013

The primary renal arteries transport up to one fourth of cardiac output to the kidneys for blood plasma ultrafiltration, with a functional dependence on the vessel geometry, composition and mechanical properties. Despite the critical physiological function of the renal artery, the few biomechanical studies that have focused on this vessel are either uniaxial or only partially describe its bi-axial mechanical behavior. In this study, we quantify the passive mechanical response of the primary porcine renal artery through bi-axial mechanical testing that probes the pressure-deformed diameter and pressure-axial force relationships at various longitudinal extensions, including the *in-vivo* axial stretch ratio. Mechanical data are used to parameterize and validate a structure-motivated constitutive model of the arterial wall. Together, experimental data and theoretical predictions of the stress distribution within the arterial wall provide a comprehensive description of the passive mechanical response of the porcine renal artery.

Keywords: Arterial mechanics; constitutive model; elasticity; thick-walled; stress.

1. Introduction

Renal vascular disease (RVD) occurs in approximately 7% of the elderly population, potentially causing stenosis, renovascular hypertension, chronic renal insufficiency, or end-stage renal disease.[1–3] In addition to compromising kidney function, RVD can incite systemic disorders, including impairments of acid-base blood balance,

‡Corresponding author.

electrolyte concentrations and extracellular fluid volume.[3–7] Due to the critical nature of kidney physiologic function and the impact on overall health, there is a pressing need for comprehensive studies of the mechanical behavior of the renal artery.

Arterial mechanical behavior depends on the geometry of the vessel, residual strains that exist in the state of no load, composition of arterial wall and mechanical properties of the major load bearing constituents. Because vascular cells are mechanosensitive, vascular homeostasis requires that stresses in the arterial wall are kept at preferable baseline values via an acute vasomotor response to transient alterations or an adaptive remodeling response to sustained changes in pressure and blood flow.[8–13] The deformed arterial dimensions can be measured during *in-vitro* or *in-vivo* experiments and the average circumferential stress in the arterial wall can be calculated from the conditions of overall equilibrium. However, this information is not sufficient for understanding normal and pathological arterial function. Evaluation of the contributions of geometry and mechanical properties to the mechanical behavior, quantification of the stress distribution in the arterial wall and prediction of the outputs of arterial remodeling require building predictive mathematical models of the arterial response. Proposing such models necessitates a constitutive formulation of arterial tissue in terms of continuum mechanics.

It has gained acceptance that the constitutive formulation of the passive mechanical properties of arterial tissue, i.e., when the effects of activated smooth muscle cells are neglected, can be performed in the framework of the theory of non-linear elastic solids. The constitutive stress–strain relations are derived from a strain energy density function (SEF), the analytical form and material constants of which are determined from at least two-dimensional mechanical tests. Three approaches for determination of arterial tissue SEFs have been proposed to date. Phenomenological models propose a SEF functional form with material constants identified based on a best fit between experimentally recorded data and corresponding theoretical predictions.[14–17] While phenomenological models can accurately match experimental data, they do not account for the contribution of the tissue structural and compositional features that give rise to the observed mechanical behavior. Conversely, structure-motivated models adopt an analytical form of the SEF that is selected in keeping with the facts that elastin is the major load bearing structural component at low strains while the stiffer collagen fibers are gradually recruited as strains increase.[18–20] Finally, structural-based models result in identification of SEFs that explicitly account for the individual mechanical properties and the amount of the structural load-bearing constituents.[21–24] Thus, parameter identification for structure-based models entails not only finding a best-fit of theoretical predictions to experimentally recorded mechanical data, but also the incorporation of compositional parameters that account for the mass fractions of load bearing constituents in the arterial wall.

Porcine arterial tissues are commonly used to evaluate the mechanical response of various vessel types due to similarities with human tissue, typical availability,

and the ability to generate relevant animal models for systematic study of induced disease states, such as hypertension, atherosclerosis, and aneurysm formation. Published investigations on various porcine arteries include the iliac,[25] basilar,[26] right and left coronary,[27] left circumflex,[28] and ascending, descending and abdominal aorta.[29] Among these and other studies, significant ranges of vessel properties have been reported, such as a mean circumferential stress at physiological load of 40.3 kPa in the coronary[30] up to 229 kPa in the iliac artery,[25] and *in-situ* axial stretch 1.17 in the basilar artery[26] up to 1.41 in the left circumflex artery.[28]

Surprisingly, among the numerous mechanical investigations devoted to large blood vessels, only few deal with renal arteries.[31,32] This study focuses on the description of the renal artery passive mechanical response, including a constitutive formulation of the tissue and evaluation of the stress distribution throughout the wall. Because the active response manifests on the background of the passive response, the first step toward a complete quantification of renal artery mechanics is determination of the latter, when the effect of the smooth muscle contraction/relaxation is not taken into account.[33] In this study we apply an integrated experimental-theoretical approach to quantify the passive mechanical response of the primary porcine renal artery and propose a structure-motivated constitutive formulation of the arterial tissue.

2. Materials and Methods

2.1. *Vessel isolation*

All tissue handling protocols were approved by the Institutional Animal Care and Use Committee at the University of South Carolina. The experimental sample set included six primary porcine renal arteries, which were harvested from the right kidney of six male Landrace Pigs (age 8–12 months, mass 60–70 kg). All kidneys were acquired immediately after animal sacrifice and placed on ice for transport to the laboratory. Upon kidney arrival, the primary renal artery was isolated from the surrounding tissue, washed in phosphate buffered saline (PBS), dissected free of perivascular tissue and mounted on stainless steel cannulae for mechanical testing. Samples were not frozen during transportation and less than one hour passed from the time of animal sacrifice to the initiation of mechanical testing. The *in-situ* axial stretch ratio $\lambda_{in\text{-}situ}$ of each sample was calculated based on the relative lengths of a vessel segment prior to and following excision. Similar methodologies for tissue extraction and handling have been previously incorporated into passive mechanical studies of vascular tissue.[34,35]

2.2. *Zero-stress configuration*

Quantification of the strains due to deformation of an artery requires specification of the geometry of the arterial cross-section in the state of no stress. It is well-established that the zero-stress configuration of an artery is obtained after a radial cut on

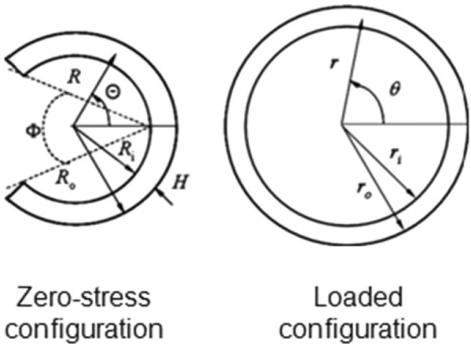

Fig. 1. Schematics of the idealized geometries of the (a) zero-stress and (b) deformed arterial configurations.

an unloaded ring segment.[36] The segment takes a form close to a circular sector, and thus is characterized by the opening angle (Fig. 1(a)). The zero-stress configurations of opened-up ring segments were quantified by measures of the inner L_i and outer L_o arc lengths and cross-sectional area A via analytical microscopy. The image analysis software Image-Pro 6.0 was used to quantify the geometry of the opened-up ring configuration. Images were acquired with a Nikon Coolpix s3500 digital camera with resolution of 20 microns/pixel. Sample arc lengths and cross-sectional area were measured by counting the number of pixels along and between the inner and outer surfaces of the sector and comparing to a reference length.

After some simple algebraic manipulation, the wall thickness H and opening angle Φ are calculated as follows[37]:

$$H = \frac{2A}{L_i + L_o}, \quad \Phi = \pi - \frac{L_o - L_i}{2H}. \tag{1}$$

2.3. *Mechanical testing*

Arterial segments were mounted onto stainless steel cannulas and secured within a chambered vascular testing system (Bose BioDynamic 5270) via sterile suture (Fig. 2). The testing system and automated system software (Wintest) were used to impart luminal flow and axial stretch to arterial samples submerged in PBS. Luminal pressure was controlled via restriction of flow distal to the arterial sample and measured by a catheter-based pressure transducer located at the flow inlet of the arterial sample, while axial stretch was controlled via programmed displacement of one end of the vessel. At each prescribed experimental state (luminal pressure and axial stretch), the axial force response was measured by a load cell aligned with the sample longitudinal axis (50 measurements/sec), and the vessel outer diameter was measured with an external camera integrated into the system via LabVIEW (5 measurements/sec).

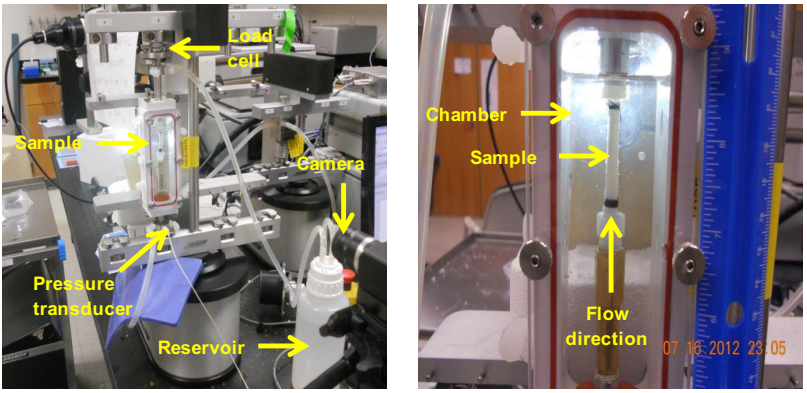

(a) (b)

Fig. 2. (Color online) The experimental set-up used for mechanical testing. (a) The overall set-up included a load cell to measure axial force, a pressure transducer to measure luminal pressure, and a mounted camera to measure external diameter. (b) The vessel was maintained in a chamber throughout testing, with a luminal flow established in the indicated direction.

Arterial segments were extended to the *in-situ* length and preconditioned with four inflation/deflation cycles (pressure range 0–250 mmHg) to obtain an elastic pressure-diameter response. Segments were then extended and pressurized at fixed lengths that yield four axial stretch ratios ranging from 90% to 120% of the *in-situ* value. To realize a quasi-static inflation at a given axial stretch that spans the *in-vivo* pressures in a pig (systolic pressure 151 ± 10 mmHg, diastolic pressure 108 ± 9 mmHg, mean pressure 129 ± 11.5),[38] the segments were pressurized up to 250 mmHg with 25 mmHg steps at a step rate of 2 mmHg/second. Sample pressurization was achieved within an open flow system, such that there is no direct contribution of luminal pressure to the measured axial force. The average axial force and outer vessel diameter were recorded over a 30 s interval for each experimental state (pressure and axial stretch ratio). Each arterial sample was tested three times following the above protocol, with the omission of preconditioning in the second and third trials. Mechanical response variables were reported as an average and standard deviation of values obtained in the three trials. The described procedure for isolation and mechanical testing of a given vessel required a total of 2 h, thus minimizing the effect of tissue degradation on the acquired data.

2.4. *Histological analysis*

Following mechanical testing, five ring samples (1 mm thick) from each arterial test segment were paraffin-embedded and processed with standard Verhoeff–Van Gieson and picrosirius red staining protocols.[39] Image analysis of histological slides was used to estimate the dry mass fractions of elastin and collagen within each segment. All histological image analyses were performed via histogram-based image

segmentation in Image Pro 6.0. To detect collagen content, picrosirius red staining density was quantified in hue-saturation-intensity (HSI) mode, with settings of H: 0–255, S: 0–255 and I: 55–254. To detect collagen content, Verhoeff–Van Geison staining density was quantified in red–green–blue (RGB) mode, with settings of: 0–255, G: 0–255 and B: 0–179. Total sample area was measured in HSI mode, with settings of H: 0–255, S: 0–255 and I: 0–254. The spatial resolution of all images was 0.752 pixels/micron in both the x-direction and y-direction. Average values of collagen and elastin content were calculated for each vessel and expressed as a percentage of total vessel dry mass.[40]

2.5. *Data analysis*

As a result of applied loads, the vessel deforms and the arterial cross-section takes a form close to a circular ring (Fig. 1(b)). The data recorded during mechanical testing are the deformed outer diameter d_o and the axial force F. Making use of the assumption of vessel incompressibility,

$$r_i = \sqrt{r_o^2 - \frac{A}{\pi\lambda_z}}, \tag{2}$$

where r_o and r_i are the deformed inner and outer radii, respectively.

Conditions of the overall equilibrium of the deformed arterial segment allow calculating the average circumferential and axial stresses as follows[9]:

$$\langle\sigma_\theta\rangle = \frac{Pr_i}{r_o - r_i}, \quad \langle\sigma_z\rangle = \frac{F}{\pi(r_o^2 - r_i^2)}. \tag{3}$$

Hereafter the subscripts θ and z refer to the circumferential and axial directions, respectively.

The average circumferential stretch ratio is:

$$\langle\lambda_\theta\rangle = \frac{2\pi(r_i + r_o)}{L_i + L_o}. \tag{4}$$

Finally, the experimentally recorded data allow calculating the pressure-diameter modulus, also called the Peterson's modulus, which characterizes the linearized mechanical response of the artery around a certain deformed state. Peterson's modulus E_p is calculated as:

$$E_P = \frac{r_o \Delta P}{\Delta r_0}, \tag{5}$$

where Δr_0 is the small increase in outer radius due to small increase in pressure ΔP.[41]

2.6. *Constitutive framework*

The renal artery is considered as a 3-D thick-walled cylindrical tube, which under applied pressure and longitudinal extension experiences a finite elastic deformation

and is in an axisymmetric deformed state. The passive mechanical properties of the vascular tissue depend on the properties, amount and spatial arrangement of elastin and collagen, which are the major load bearing structural constituents; the contribution of the vascular smooth muscle cells to the passive response is neglected. The solution of the boundary value problem of the vessel mechanical response can be found in several theoretical studies in vascular solid mechanics.[9,37]

Arterial deformation is characterized by the right Cauchy–Green strain tensor

$$[C] = \text{diag}\{\lambda_r^2, \lambda_\theta^2, \lambda_z^2\} = \text{diag}\left\{\left(\frac{dr}{dR}\right)^2, \left(\frac{\chi r}{R}\right)^2, \lambda_z^2\right\},$$
$$\chi = \frac{\pi}{\pi - \Phi}, \quad \lambda_z = \frac{l}{L}, \tag{6}$$

where r and R are the radial coordinates of an arbitrary point within the arterial wall before and after deformation (Fig. 1); L and l are the length of the arterial segment before and after deformation.

Because of material incompressibility

$$\frac{dr}{dR}\frac{r}{R}\chi\lambda_z = 1, \tag{7}$$

which after integration yields

$$r = \sqrt{r_o^2 - \frac{1}{\chi\lambda_z}(R_o^2 - R^2)}. \tag{8}$$

Equations (7) and (8) show that the components of the strain tensor are completely described if the zero-stress configuration, axial stretch ratio λ_z and deformed outer radius r_o are known.

We adapt the analytical form of the strain energy density function W motivated by the structure of arterial wall proposed in Ref. 42.

$$W = c\,(I_1 - 3) + \sum_{k=1,2,3,4} \frac{b_{1k}}{4b_{2k}}\{\exp[b_{2k}(\lambda_k^2 - 1)^2] - 1\}. \tag{9}$$

The first term accounts for contribution of the elastin. c is a material constant, and $I_1 = \lambda_\theta^2 + \lambda_z^2 + (\lambda_\theta\lambda_z)^{-2}$ is the first invariant of the strain tensor. The second term includes the contribution of four families of collagen fibers. Subscript k denotes a family of collagen fibers oriented at a mean angle of α_k with respect to the longitudinal vessel axis; b_{1k}, and b_{2k} are material constants and $\lambda_k = \sqrt{\lambda_\theta^2 \sin^2\alpha_k + \lambda_z^2 \cos^2\alpha_k}$ is the stretch ratio of each family of collagen fibers due to deformation.

Given the strain energy function W, the Cauchy stress tensor $[\mathbf{T}]$ is

$$[T] = \text{diag}\{\sigma_r, \sigma_\theta, \sigma_z\} = \text{diag}\left\{-p, \lambda_\theta\frac{\partial W}{\partial \lambda_\theta} - p, \lambda_z\frac{\partial W}{\partial \lambda_z} - p\right\}, \tag{10}$$

where p is unknown function due to the material incompressibility. Making use of equations of equilibrium and the boundary conditions that the arterial segment is

inflated by an applied internal pressure which is equal to the radial stress at the inner surface, while outer surface is traction free, and that the resultant of the axial stress is equal to the measured axial force, the stress components are[9]

$$\sigma_r = \int_{r_i}^{r} \lambda_\theta \frac{\partial W}{\partial \lambda_\theta} \frac{dr}{r} - P, \quad \sigma_\theta = \sigma_r + \lambda_\theta \frac{\partial W}{\partial \lambda_\theta}, \quad \sigma_z = \sigma_r + \lambda_z \frac{\partial W}{\partial \lambda_z}. \tag{11}$$

Given the segment zero-stress state dimensions L_i, L_o, Φ and strain energy function W, any deformed configuration characterized by the outer deformed radius r_o and axial stretch ratio λ_z is realized by applying pressure and axial force as follows[9]:

$$P = \int_{r_i}^{r_o} \lambda_\theta \frac{\partial W}{\partial \lambda_\theta} \frac{dr}{r}, \quad F = \pi \int_{r_i}^{r_o} \left(2\lambda_z \frac{\partial W}{\partial \lambda_z} - \lambda_\theta \frac{\partial W}{\partial \lambda_\theta} \right) r dr + \pi r_i^2 P. \tag{12}$$

Equations (6)–(12) can be used for determining the values of the material constants of the strain energy function associated with arterial tissue subjected to an inflation-extension test. Considering the material constants c, b_{1k}, b_{2k} as unknown parameters, their values are determined by the minimization of the following objective function

$$\Omega = w_1 \sum_{n=1}^{N} \left(\frac{P_n^T - P_n^E}{P_n^E} \right)^2 + w_2 \sum_{n=1}^{N} \left(\frac{F_n^T - F_n^E}{F_n^E} \right)^2, \tag{13}$$

where the superscript E and T refer to the experimentally recorded and theoretically calculated values of the pressure and axial force, and subscript n indicates a particular experimental state; w_1 and w_2 are weighting coefficients, such that $w_1 + w_2 = 1$. To be thermodynamically admissible, the contour of the curves $W(\lambda_\theta, \lambda_z) = \text{const}$ on the $(\lambda_\theta, \lambda_z)$ plane must be convex for all values of material constants. The magnitude of the objective function Ω serves as quantitative measure for the "goodness" of the theoretically predicted loads.

After minimization of Ω and identification of the constants of W, Eqs. (6)–(12) can be used to calculate the model predictions for the deformed configurations, average circumferential and axial stress and stress distribution across the arterial wall for any loading scenarios characterized by the values of applied pressure P and axial stretch ratio λ_z.

3. Results

3.1. *Zero-stress configuration*

The zero-stress configuration of the porcine renal artery was determined via image analysis of an opened-up ring segment (Table 1). The average values obtained among six vessels for inner L_i and outer L_o arc lengths and cross-sectional area A were 13.4 ± 2.8 mm, 17.3 ± 2.4 mm and 17.8 ± 0.9 mm^2, respectively. The thickness and opening angle of each idealized sector was calculated based on these measurements, with average values of 1.16 ± 0.33 mm and $84.0 \pm 12.4°$.

Table 1. The zero-stress configuration for each arterial test segment. R_i, H, Φ, L_i, L_o and A are the inner radius, wall thickness, opening angle, inner arc length, outer arc length and cross-sectional area, respectively.

Vessel	R_i [mm]	H [mm]	Φ [°]	L_i [mm]	L_o [mm]	A [mm^2]
1	4.58	1.47	82.55	15.59	20.59	26.61
2	4.41	1.47	105.48	11.47	15.29	19.69
3	3.04	1.29	79.68	10.65	15.16	16.64
4	2.99	1.21	72.52	11.21	15.76	16.34
5	5.70	0.63	90.58	17.78	19.75	11.88
6	3.71	0.90	73.43	13.79	17.13	13.89
Avg.	4.07	1.16	84.04	13.41	17.28	17.84
Std. Dev.	1.04	0.33	12.40	2.83	2.36	0.87

3.2. *Arterial wall composition*

The dry mass fractions of elastin and collagen in the arterial wall were determined via histological staining and image analyses (Fig. 3). Elastin had an average mass fraction of $12.6\% \pm 1.87\%$ and was primarily concentrated in the internal elastic lamina. Collagen had an average mass fraction of $36.4\% \pm 6.78\%$, with a relatively greater concentration in the adventitia as compared to the media.

3.3. *Experimentally recorded mechanical response*

Quasi-static inflation-extension tests generated bi-axial data describing the passive mechanical response of the primary porcine renal artery. The pressure-deformed diameter relationships exhibited non-linearity over the examined pressure range at all levels of fixed axial stretch, characterized by a steepening of the curves at higher pressures (Fig. 4). Peterson's modulus E_p was calculated for each vessel at physiologic loading conditions ($P = 13.33\,\text{kPa}$, $\lambda_z = \lambda_{in\text{-}situ}$), with an average value of $251.3 \pm 133.5\,\text{kPa}$.

An increase in pressure generally caused an increase in the axial wall force at axial stretch ratios at or above the *in-situ* value, while an inverse trend was exhibited at low pressures (Fig. 5). Vessel bucking was induced at higher pressures when the axial stretch ratio was below the *in-situ* value, which concurs with findings of several theoretical and experimental studies.[43–45] The occurrence of buckling confounded experimental measurements and required the exclusion of corresponding data from the mechanical testing data set. Increased axial stretch resulted in higher axial force at all pressures.

3.4. *Parameter identification*

The parameter values for the proposed constitutive model were identified via a Levenberg–Marquardt non-linear least squared method for minimization of the objective function Ω. The weighting coefficients w_1 and w_2 were taken to be 0.5 in order to yield theoretical predictions which agreed well with both recorded pressures

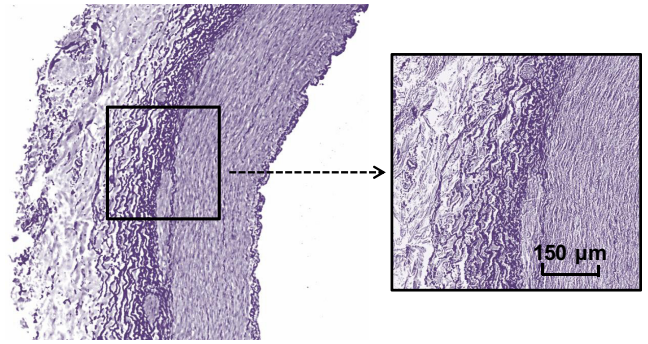

(a)

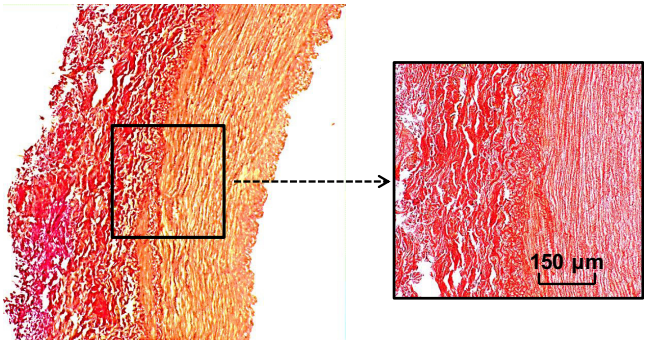

(b)

Fig. 3. (Color online) Representative histological images of the porcine renal artery wall viewed at 40× magnification. (a) Elastin is black under Verhoeff–Van Gieson staining, while (b) collagen is pink/red under picrosirius red staining.

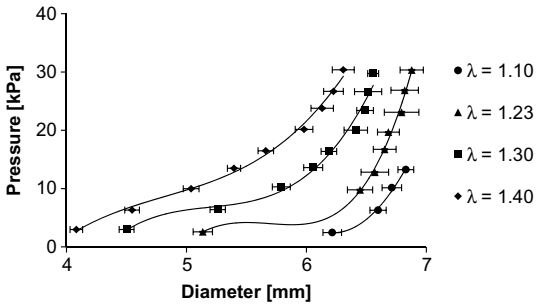

Fig. 4. Representative data for the pressure-deformed outer diameter relationship of the porcine renal artery at three levels of axial stretch (1.1, 1.23 and 1.3). Data points represent mean values ($n = 3$); error bars denote standard deviation.

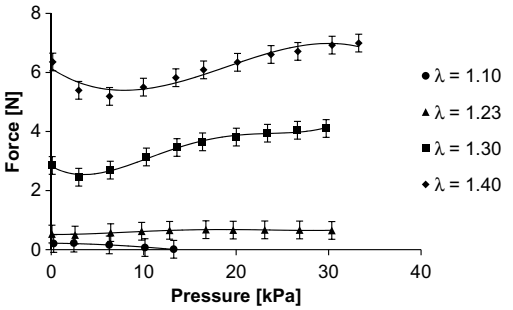

Fig. 5. Representative data for the axial wall force-pressure relationship of the porcine renal artery at three levels of axial stretch (1.1, 1.23 and 1.3). Data points represent mean values ($n = 3$); error bars denote standard deviation.

Table 2. Best-fit parameters and corresponding residual values for the structure-motivated model of the renal artery.

Vessel	c [kPa]	b_{11} [kPa]	b_{12}	b_{21} [kPa]	b_{22}	b_{31} and b_{41} [kPa]	b_{32} and b_{42}	α_1 [deg]	α_2 [deg]	α_3 [deg]	α_4 [deg]	Residual
1	5.05	3.01	0.48	54.74	0.93	6.99	6.89	90	0	57.69	−57.69	0.70
2	19.38	6.66	6.15	0.50	4.60	6.11	6.90	90	0	46.36	−46.36	1.49
3	0.53	17.63	6.57	9.12	5.48	35.98	1.91	90	0	34.84	−34.84	0.60
4	0.52	15.95	7.89	9.69	3.56	33.55	3.02	90	0	42.23	−42.23	1.05
5	0.51	45.49	6.21	14.57	4.60	5.61	6.26	90	0	89.96	−89.96	1.30
6	2.68	5.01	6.22	15.98	2.55	7.67	4.31	90	0	38.06	−38.06	1.91
Avg.	4.78	15.62	5.59	17.43	3.62	15.99	4.88	90	0	51.52	−51.52	1.18
Std. Dev.	7.38	15.80	2.59	19.07	1.66	14.59	2.13	0	0	20.43	20.43	0.49

and axial forces. The obtained residual values correspond to acceptable fits between experimental and theoretical data (Table 2).

3.5. *Model validation*

Model predictions for the pressure-diameter (Fig. 6(a)) and force-axial stretch (Fig. 6(b)) relationships of the renal artery agreed well with experimental data over the examined range of mechanical behavior. Moreover, predicted mean stress versus stretch curves in the circumferential (Fig. 7(a)) and axial (Fig. 7(b)) directions also agreed with the measured mechanical response. The thermodynamic admissibility of the identified strain energy function was verified via plotting of selected values as a function of deformation variables. The convexity of the resultant curves indicated a reasonable solution (Fig. 8).

3.6. *Wall stress distribution*

The model was used to predict the circumferential stress distribution across the arterial wall thickness (Fig. 9(a)). Under loads close to physiologic conditions

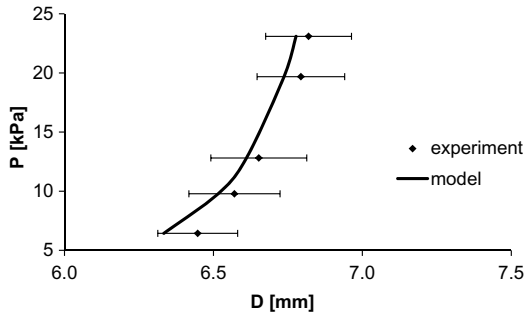

(a)

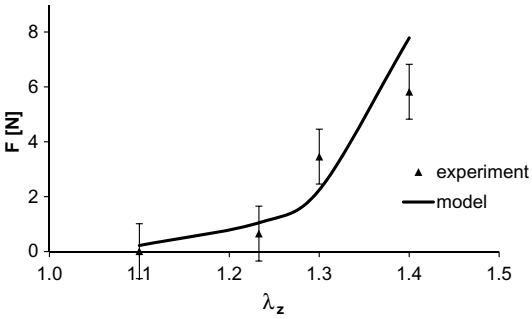

(b)

Fig. 6. Representative comparison of experimental values (data points) and theoretical predictions (curves) for the (a) pressure-deformed outer diameter and (b) wall force-axial stretch ratio relationships of the porcine renal artery. Error bars denote standard deviation of experimental measurements ($n = 3$).

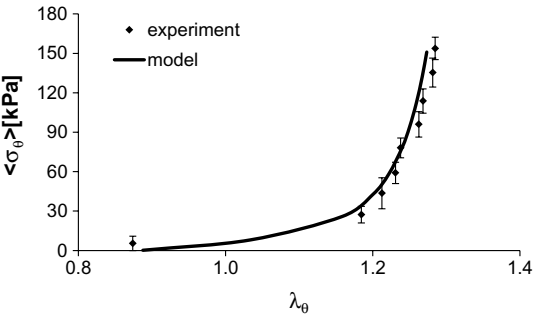

(a)

Fig. 7. Representative comparison of experimental values (data points) and theoretical predictions (curves) for the (a) mean circumferential stress-circumferential stretch ratio and (b) mean axial stress-axial stretch ratio relationships of the porcine renal artery. Error bars denote standard deviation of experimental measurements ($n = 3$).

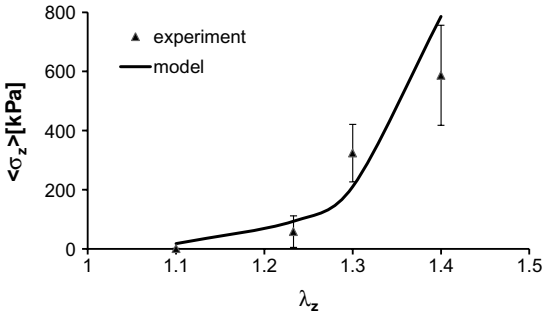

(b)

Fig. 7. (*Continued*)

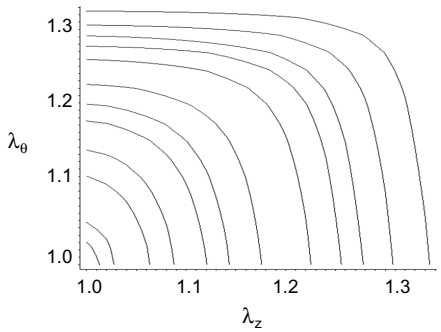

Fig. 8. Contour curves of $W(\lambda_\theta, \lambda_z) = \text{const}$ on the $(\lambda_\theta, \lambda_z)$ plane. The convexity of the curves guarantees the thermodynamically admissibility of W.

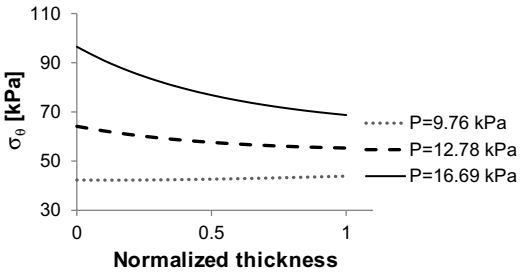

(a)

Fig. 9. (a) Representative predictions of circumferential stress throughout the arterial wall at the *in-situ* axial stretch ratio (1.23) and pressures of 9.76, 12.78 and 16.69 kPa. (b) Representative predictions of circumferential stress distribution at fixed pressure (13.33 kPa) and axial stretch ratios of 1.1, 1.23 and 1.3. In both plots, the radial position has been normalized such that 0 and 1 refer to the inner and outer deformed radii, respectively.

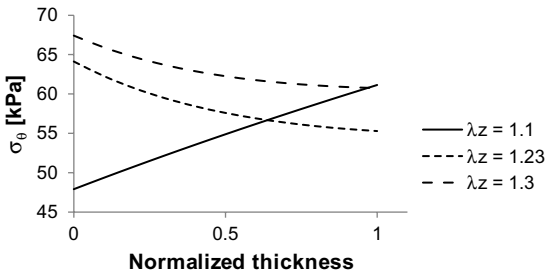

(b)

Fig. 9. (*Continued*)

($\lambda_z = \lambda_{in\text{-}situ}$, $P \approx 100$ mmHg), the circumferential stress was maximal at the inner surface and decreased with increasing radial position. The stress distribution was qualitatively reversed when $\lambda_z < \lambda_{in\text{-}situ}$, as circumferential stress increased with radial position (Fig. 9(b)).

4. Discussion

The aim of this study was to quantify the passive mechanical response of the primary porcine renal artery and develop a mathematical model that facilitates calculation of arterial wall stresses and strains under physiologic loading. The obtained results can be sorted according to their descriptive and predictive characteristics. The passive mechanical response is *described* in terms of the internal pressure-deformed diameter and internal pressure-axial force relationships at fixed arterial lengths. Moreover, data are processed to calculate parameters that *describe* a local linearized measure of the mechanical response, namely the pressure-diameter modulus in the neighborhood of physiologic loading conditions. A structure-motivated constitutive model of the renal artery was proposed and validated to allow solving boundary-value problems, the solutions of which *predict* arterial response and wall stress distribution under different loading scenarios.

Some data recorded in this study are within the range of published results for other types of porcine arteries. The opening angle characterizing the zero-stress configuration of the renal artery was found to be $84.0° \pm 12.4°$, which is similar to values reported for the porcine carotid ($84.7° \pm 9°$) and left circumflex ($75° \pm 29°$) arteries.[28,46] Experimental results show a non-linearity of the pressure-deformed diameter relationship, which is commonly observed and attributed to the non-linear mechanical response of elastin and the gradually increased load-bearing of collagen fibers as they straighten out at higher pressures. However, despite general similarity with mechanical data on large conduit vessels, the pressure-deformed diameter curve of the primary renal artery does not exhibit the typical convex portion over the range of low pressures as reported for porcine abdominal aorta[29] and carotid

arteries.[46] It gained acceptance that the convex shape of the low pressure response is mainly due to the contribution to elastin in load bearing. As a typical muscular vessel the renal artery exhibits low elastin content. The dry mass fraction obtained for elastin obtained in this study for the primary porcine renal artery, namely $12.6\% \pm 1.87\%$, is below the 19–53% range reported for the porcine carotid artery[46] but close to $18.7\% \pm 1.8\%$ reported for the canine renal artery.[47] Therefore it is reasonable to speculate that the reported shape of the passive pressure-deformed diameter curves (Fig. 4) is due to low elastin content. A similar difference in the passive mechanical response of a muscular artery (rabbit basilar artery) and an elastic artery (rabbit common carotid) was reported in Ref. 40. Another possibility that might explain the passive mechanical response of the porcine primary renal artery is a less wavy unloaded configuration of collagen fibers, and their involvement into load-bearing even at low pressures. Detailed histological assessment of the distribution and configuration of collagen fibers within arterial wall in the state of zero stress could be conducted with multi-photon microscopy and could test these speculations.[47,48]

The pressure-diameter modulus of the renal artery near physiologic loading conditions is 251.3 ± 133.5 kPa, which is significantly greater than the value reported for the same vessel *in-vivo* (24 ± 1 kPa).[14] The discrepancy between renal artery Peterson's modulus *in-vivo* and *in-vitro* as calculated in the present study might be due to the contribution of the basal vascular tone, which is expected to be significant in muscle-type vessels but only accounted for with *in-vivo* measurements. Contraction of the vascular smooth muscle reduces the deformed diameter of the vessel and circumferential stretch ratio, which in turn decreases the structural stiffness due to the non-linearity of the mechanical response.

The limitations of this study are associated with the introduced assumptions. The variation of collagen fiber orientation is only partially accounted for by the four fiber constitutive model, while there is in fact a continuous distribution of fiber orientations. Moreover, the proposed one-layered model assumes that the arterial wall composition and structure are uniform in the radial direction. More detailed assessment of arterial wall composition and structure may impact theoretical predictions of the stress–strain relationships and better attribute the mechanical response to individual load-bearing constituents.

Quantifying the passive mechanical properties is a requisite step to understanding the primary determinants of renal artery mechanical performance. Subsequent studies that probe the SMC-mediated active mechanical response, the baroreceptor-mediated response to arterial pressure and the endothelial-cell mediated response to shear, will together elucidate the renal artery mechanical response in conditions of health and disease. Additional histological studies could provide insight into the microstructural configuration of collagen within the arterial wall, and help explain the particular shape of the obtained pressure-deformed diameter response curves.

5. Conclusion

In both basic science and clinical research, including disease diagnosis, cellular signal mechanotransduction and vascular tissue engineering, it is advantageous to understand the arterial mechanical response under various loading conditions and states of health. Accordingly, one of the major objectives of vascular biomechanics is the determination of the constitutive equations that describe tissue mechanical properties and allow formulating and solving boundary value problems with predictive power. In the presented study, bi-axial mechanical testing coupled with structure-motivated constitutive modeling enabled quantification of the passive mechanical response of the primary porcine renal artery, including assessment of the stresses experienced by vascular cells within the arterial wall. Quantifying the passive mechanical response of renal arteries is a necessary step to understanding physiological and pathophysiological mechanical performance, and may provide insight into the genesis and progression of certain forms of RVD.

Acknowledgments

This work was supported by the National Science Foundation/EPSCoR Grant to T.S. (EPS-0903795).

References

1. Adamczak M, Wiecek A, The management of atherosclerotic renovascular disease, *Kidney Blood Press Res* **34**(4):277–283, 2011.
2. Edwards MS, Corriere MA, Contemporary management of atherosclerotic renovascular disease, *J Vasc Surg* **50**(5):1197–1210, 2009.
3. Wright JR, Shurrab AE, Cooper A, Kalra PR, Foley RN, Kalra PA, Progression of cardiac dysfunction in patients with atherosclerotic renovascular disease, *Qjm* **102**(9):695–704, 2009.
4. Cheung CM, Wright JR, Shurrab AE, Mamtora H, Foley RN, O'Donoghue DJ *et al.*, Epidemiology of renal dysfunction and patient outcome in atherosclerotic renal artery occlusion, *J Am Soc Nephrol* **13**(1):149–157, 2002.
5. Chrysochou C, Kalra PA, Current management of atherosclerotic renovascular disease — what have we learned from ASTRAL? *Nephron Clin Pract* **115**(1):c73–c81, 2010.
6. Davis RP, Pearce JD, Craven TE, Moore PS, Edwards MS, Godshall CJ *et al.*, Atherosclerotic renovascular disease among hypertensive adults, *J Vasc Surg* **50**(3):564–570, 2009.
7. Hillege H, Van Gilst W, de Zeeuw D, van Veldhuisen DJ, Renal function as a predictor of prognosis in chronic heart failure, *Heart Fail Monit* **2**(3):78–84, 2002.
8. Mullen M, Heterogeneous nature of flow-mediated dilatation in human conduit arteries *in vivo*: Relevance to endothelial dysfunction in hypercholesterolemia, *Circul Res* **88**:145–151, 2001.
9. Humphrey JD, *Cardiovascular Solid Mechanics* (Springer-Verlag, New York, 2002).
10. Kamiya A, Togawa T, Adaptive regulation of wall shear stress to flow change in canine carotid artery, *Am J Physiol* **239**:14–21, 1980.

11. Langille BL, Blood flow-induced remodeling of the artery wall, in Bevan JA, Kaley G, Rubanyi G (eds.), *Flow-Dependent Regulation of Vascular Function*, Oxford University Press, New York, pp. 227–299, 1995.
12. Liu SQ, Fung YC, Relationship between hypertension, hypertrophy and opening angle of zero-stress state of arteries following aortic constriction, *J Biomech Eng* **111**:325–335, 1989.
13. Matsumoto T, Hayashi K, Stress and strain distribution in hypertensive and normotensive rat aorta considering residual strain, *J Biomech Eng* **118**:62–73, 1996.
14. Rachev A, Theoretical study of the effect of stress dependent remodeling on arterial geometry under hypertensive conditions, *J Biomech* **30**:819–827, 1997.
15. Rachev A, A model of arterial adaptation to alterations in blood flow, *J Elast* **61**:83–111, 2000.
16. Rachev A, Stergiopulos N, Meister JJ, Theoretical study of dynamics of arterial wall remodeling in response to changes in blood pressure, *J Biomech* **29**:635–642, 1996.
17. Rachev A, Stergiopulos N, Meister JJ, A model for geometrical and mechanical adaptation of arteries to sustained hypertension, *J Biomech Eng* **120**:9–17, 1998.
18. Taber LA, Humphrey JD, Stress-modulated growth, residual stress, and vascular heterogeneity, *J Biomech Eng* **123**:528–535, 2001.
19. Tsamis A, Stergiopulos N, Arterial remodeling in response to increased blood flow using a constituent-based model, *J Biomech* **42**:531–536, 2009.
20. Tsimas A, Stergiopulos N, Rachev A, A structure-based model of arterial remodeling in response to sustained hypertension, *J Biomech Eng* **131**:101004-1–101004-8, 2009.
21. Alford PW, Humphrey JD, Taber LA, Growth and remodeling in a thick-walled artery model: Effects of spatial variations in wall constituents, *Biomech Model Mechanobiol* **7**:245–262, 2008.
22. Gleason RL, Humphrey JD, Effects of a sustained extension on arterial growth and remodeling: A theoretical study, *J Biomech* **38**:1255–1261, 2005.
23. Gleason RL, Humphrey JD, A 2-D constrained mixture model for arterial adaptations to large changes in flow, pressure, and axial stretch, *Math Med Biol* **22**:347–369, 2005.
24. Gleason RL, Taber LA, Humphrey JD, A 2-D model of flow-induced alterations in the geometry, structure, and properties of carotid arteries, *J Biomech Eng* **126**:371–381, 2004.
25. Mekkaoui C, Friggi A, Rolland PH, Bodard H, Bartoli JM, Mesana T, Simultaneous measurements of arterial diameter and blood pressure to determine the arterial compliance, wall mechanics, and stresses *in vivo*, *Eur J Vasc Endovasc Surg* **21**:208–213, 2001.
26. HU JJ, Fossum TW, Miller MW, XU H, Liu JC, Humphrey JD, Biomechanics of the porcine basilar artery in hypertension, *Ann Biomed Eng* **35**(1):19–29, 2007.
27. Liu Y, Dang C, Garcia M, Gregersen H, Kassab G, Surrounding tissues affect the passive mechanics of the vessel wall: Theory and experiment, *Am J Physiol Heart Circ Physiol* **293**:H3290–H3300, 2007.
28. Carboni M, Desch GW, Weizsacker HW, Passive mechanical properties of porcine left circumflex artery and its mathematical description, *Med Eng Phys* **29**:8–16, 2007.
29. Han HC and Fung YC, Direct measurement of transverse residual strains in aorta, *Am J Physiol Heart Circ* **270**:H750–H759, 1996.
30. van den Broek CN, van der Horst A, Rutten MC, van de Vosse FN, A generic constitutive model for the passive porcine coronary artery, *Biomech Model Mechanobiol* **10**:249–258, 2011.
31. Cox RH, Anisotropic properties of the canine carotid artery *in vitro*, *J Biomech* **8**(5):293–300, 1975.

32. Gandley RE, Griggs KC, Conrad KP, McLaughlin MK, Intrinsic tone and passive mechanics of isolated renal arteries from virgin and late-pregnant rats, *Am J Physiol* **273**(1 Pt 2):R22–R27, 1997.
33. Vito RP, Dixon SA, Blood vessels constitutive models 1995–2002, *Annu Rev Biomed Eng* **5**:413–439, 2011.
34. Pandit A, Lu X, Wang C, Kassab GS, Biaxial elastic material properties of porcine coronary media and adventitia, *Am J Physiol Heart Circ Physiol* **288**:2581–2587, 2005.
35. Huo Y, Cheng Y, Zhao X, Lu X, Kassab GS, Biaxial vasoactivity of porcine coronary artery, *Am J Physiol Heart Circ Physiol* **302**:2058–2063, 2012.
36. Chuong CJ, Fung YC, On residual stresses in arteries, *J Biomech Eng* **108**(2):189–192, 1986.
37. Rachev A, Remodeling of arteries in response to changes in their mechanical environment, in Holzapfel G, Ogden R (eds.), *Biomechanics of Soft Tissue in Cardiovascular Systems. CISM Courses and Lectures, Course and Lecture No. 441.* Springer, Wien New York, pp. 100–161, 2003.
38. Mekkaoui C, Friggi A, Rolland PH, Bodard H, Piquet P, Bartoli JM, Mesana T, Simultaneous measurements of arterial diameter and blood pressure to determine the arterial compliance, wall mechanics and stresses *in vivo*, *Eur J Vasc Endovasc Surg* **21**:208–213, 2001.
39. Fischer GM, Llaurado JG, Collagen and elastin content in canine arteries selected from functionally different vascular beds, *Circ Res* **19**:394–399, 1966.
40. Wagner HP, Humphrey JD, Differential passive and active biaxial mechanical behaviors of muscular and elastic arteries: Basilar versus common carotid, *J Biomech Eng* **133**(5):051009, 2011.
41. Peterson LH, Jensen RE, Parnell J, Mechanical properties of arteries *in vivo*, *Circ Res* **8**:622–639, 1960.
42. Holzapfel GA, Gasser TC, Ogden RW, A new constitutive framework for arterial wall mechanics and a comparative study of material models, *J Elast* **61**:1–48, 2000.
43. Han HC, A biomechanical model of artery buckling, *J Biomech* **40**:3672–3678, 2007.
44. Rachev A, A theoretical study of mechanical stability of arteries, *J Biomech Eng* **131**(5):0510061-10, 2009.
45. Han HC, Chesnutt JK, Garcia WJR, Liu Q, Wen Q, Artery buckling: New phenotypes, models, and applications, *Ann Biomed Eng*, doi:0.1007/s10439-012-0707-0, 2012.
46. Garcia A, Pena E, Laborda A, Lostale F, De Gregorio MA, Doblare M, Martinez MA, Experimental study and constitutive modeling of the passive mechanical properties of the porcine carotid artery and its relation to histological analysis: Implications in animal cardiovascular device trials, *Med Eng Phys* **33**:665–676, 2011.
47. Schrauwen JT, Vilanova A, Rezakhaniha R, Stergiopulos N, van de Vosse FN, Bovendeerd PH, A method for the quantification of the pressure dependent 3D collagen configuration in the arterial adventitia, *J Struct Biol* **180**:335–342, 2012.
48. Hill MR, Duan X, Gibson GA, Watkins S, Robertson AM, A theoretical and non-destructive experimental approach for direct inclusion of measured collagen orientation and recruitment into mechanical models of the artery wall, *J Biomech* **45**:762–771, 2012.